Rupture of the neck in nuclear fission*

K. T. R. Davies and R. A. Managan†
Physics Division, Oak Ridge National Laboratory, Oak Ridge, Tennessee 37830

J. R. Nix
Theoretical Division, Los Alamos Scientific Laboratory, University of California, Los Alamos, New Mexico 87545

A. J. Sierk
Kellogg Radiation Laboratory, California Institute of Technology, Pasadena, California 91125
and Theoretical Division, Los Alamos Scientific Laboratory, University of California, Los Alamos, New Mexico 87545

(Received 16 February 1977)

We introduce a degree of freedom to describe the rupture of the neck in nuclear fission and calculate the point at which the neck ruptures as the nucleus descends dynamically from its fission saddle point. This is done by mentally slicing the system into two portions at its minimum neck radius and calculating the force required to separate the two portions while keeping their shapes fixed. This force is obtained by differentiating with respect to separation the sum of the Coulomb and nuclear interaction energies between the two portions. For nuclei throughout the Periodic Table we calculate this force along dynamical paths leading from the fission saddle point. The force is initially attractive but becomes repulsive when the neck reaches a critical size. For actinide nuclei the neck radius at which rupture occurs is about 2 fm. This increases the calculated translational kinetic energy of the fission fragments at infinity relative to that calculated for scission occurring at zero neck radius. With the effect of neck rupture taken into account, we calculate and compare with experimental results fission-fragment kinetic energies for two types of nuclear dissipation: ordinary two-body viscosity and one-body dissipation.

[NUCLEAR REACTIONS, FISSION Included neck-rupture degree of freedom and calculated its effect on fission-fragment kinetic energies. Modified liquid-drop model, hydrodynamical model, nuclear viscosity, one-body nuclear dissipation.]

I. INTRODUCTION

In previous dynamical calculations of fission,[1,2] scission was defined to occur at a configuration for which the radius of the neck vanishes. However, scission should in fact occur before the nucleus reaches this limiting configuration because of the delicate balance between the Coulomb and nuclear forces during the dynamical descent from the fission saddle point. For large necks the attractive nuclear force is larger than the repulsive Coulomb force, and the nucleus is stable against neck rupture. Eventually the repulsive Coulomb force becomes larger in magnitude than the attractive nuclear force. The neck then ruptures at a nonzero radius, as illustrated in Fig. 1.

The expected size of the neck when it ruptures can be estimated on the basis of simplified geometries. For this purpose we approximate the long-range Coulomb neck-rupture force in terms of the force between two spheres situated at the centers of mass of the two portions of the system. This gives

$$F_C = Z_1 Z_2 e^2 / r^2, \tag{1.1}$$

where $Z_1 e$ and $Z_2 e$ are the charges of the two portions of the system and r is the distance between their centers of mass.

The short-range nuclear force F_n is approximated by the force per unit area $\mathfrak{F}_n$ acting between two semi-infinite distributions in contact times the neck area πr_{neck}^2. The nuclear force per unit area at contact is obtained from

$$\mathfrak{F}_n = -\partial \mathcal{E}_n(s)/\partial s \,|_{s=0}, \tag{1.2}$$

where

$$\mathcal{E}_n = -2\gamma e^{-s/\lambda} \tag{1.3}$$

is the nuclear interaction energy per unit area as a function of the separation s between the surfaces of the two-semi-infinite distributions, for a Yukawa effective two-nucleon interaction of range λ.[2-5] The surface tension γ is related to the surface-energy constant a_s, the surface-asymmetry constant κ, and the nuclear-radius constant r_0 of the semiempirical nuclear mass formula by

$$\gamma = a_s(1 - \kappa I^2)/4\pi r_0^2, \tag{1.4}$$

where $I = (N - Z)/A$ is the relative neutron excess. This gives for the total nuclear force

$$F_n = -2\pi\gamma r_{\text{neck}}^2/\lambda = -a_s(1 - \kappa I^2) r_{\text{neck}}^2/2\lambda r_0^2. \tag{1.5}$$

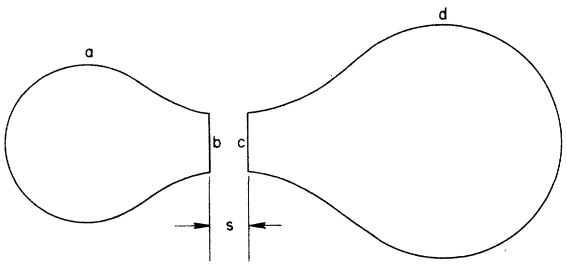

FIG. 1. Illustration of the neck-rupture degree of freedom. The nucleus is sliced into two portions at its minimum neck radius. In evaluating the interfragment forces we take the limit of $s \to 0$. The surfaces a and d refer to the curved parts of the left-hand and right-hand fragments, respectively, and b and c refer to the two flat touching faces.

The system becomes unstable against neck rupture when the Coulomb and nuclear forces are equal in magnitude, which occurs when the neck radius is

$$r_{\text{neck}} = \left(\frac{2\lambda r_0^2 Z_1 Z_2 e^2}{a_s (1 - \kappa I^2) r^2} \right)^{1/2} . \tag{1.6}$$

Evaluation of this expression for the fission of an actinide nucleus such as ^{252}Cf yields a neck radius of about 1.2 fm at which rupture should occur.[2]

Of course, the simplified geometries used in making this estimate are far from the true situation, as illustrated in Fig. 1. It is therefore of interest to develop a method for calculating the Coulomb and nuclear neck-rupture forces for actual nuclear shapes encountered in fission. For this purpose we mentally divide the system into two portions at its minimum neck radius. The forces are then calculated by differentiating the Coulomb and nuclear interaction energies with respect to separation, while holding fixed the shapes of the two portions. The interaction energies are obtained in turn by integrating the Coulomb interaction and a Yukawa effective two-nucleon interaction over each of the two portions of the nucleus.[2-4]

These ideas are used in Sec. II to derive equations for the Coulomb and nuclear interfragment forces. These forces are then combined in Sec. III with dynamical calculations of fission to calculate the radius at which the neck ruptures. This is done for two types of nuclear dissipation: ordinary two-body viscosity[2,6,7] and one-body dissipation, which arises from nucleons colliding with a moving potential wall[8-16] rather than with each other. With either type of dissipation the neck radius at rupture is found to be about 2 fm for actinide nuclei, which is somewhat larger than the simple estimate presented above. This relatively large neck-rupture radius increases somewhat the translational kinetic energy of the fission fragments at infinity compared with that calculated for a zero-neck-radius scission configuration. Section III includes a calculation of this effect, as well as a comparison of calculated and experimental fission-fragment kinetic energies for nuclei throughout the Periodic Table. In Sec. IV we summarize our study and present our conclusions.

II. INTERACTION ENERGIES AND FORCES

A. Geometry

We need first to evaluate the Coulomb and nuclear interaction energies for a shape like that shown in Fig. 1. Once these interaction energies are known as functions of the separation s between the two portions of the system, the interaction forces are given by

$$F = - \partial E(s)/\partial s \,|_{s=0} . \tag{2.1}$$

Both the Coulomb and nuclear interaction energies, as well as their sum, are of the form

$$E = \int_{V_1} \int_{V_2} f(|\vec{r}_1' - \vec{r}_2'|) d^3 r_1' d^3 r_2' , \tag{2.2}$$

where f is a scalar function of $\vec{r}_1' - \vec{r}_2'$. The vectors $\vec{r}_1'$ and $\vec{r}_2'$ are labeled explicitly in Fig. 2. Since we are evaluating an interaction energy, we impose the restriction that $\vec{r}_1'$ always lies in the left-hand body (in volume V_1) and $\vec{r}_2'$ always lies in the right-hand

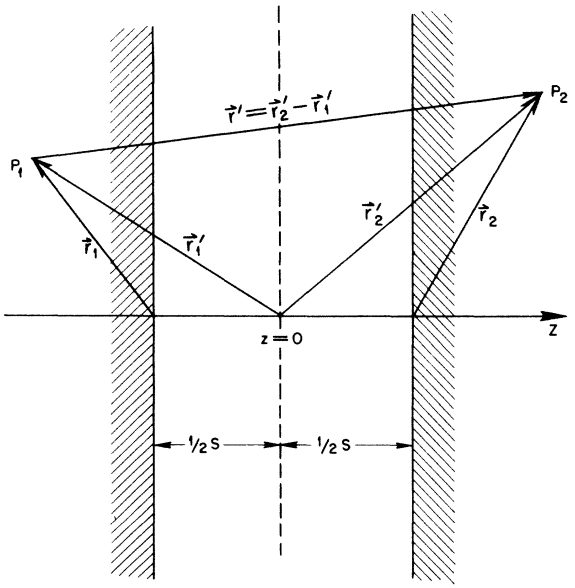

FIG. 2. Vector diagram for evaluating the interaction energies and forces for a shape like that shown in Fig. 1. The point P_1 is constrained to lie in the left-hand fragment, and the point P_2 is constrained to lie in the right-hand fragment. The shaded regions indicate the boundaries of the left-hand and right-hand fragments.

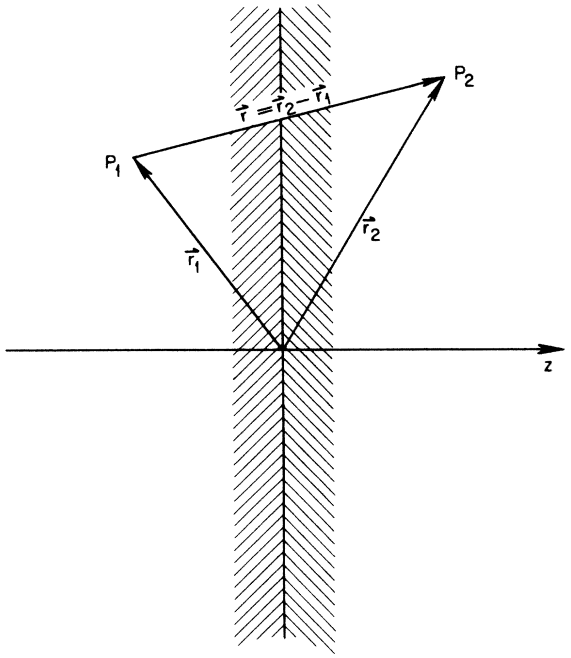

FIG. 3. The vector diagram of Fig. 2 in the limit of $s \to 0$. The points P_1 and P_2 have the same locations with respect to the boundaries of their fragments as the points P_1 and P_2 in Fig. 2. The shaded regions again indicate the boundaries of the left-hand and right-hand fragments, which are now touching.

body (in volume V_2). This restriction means that the function f occuring in Eq. (2.2) will be larger by a factor of 2 than the corresponding function in an equation for the total energy,[17] where $\vec{r}_1'$ and $\vec{r}_2'$ each vary over the entire nuclear volume.

Figure 3 shows the appearance of Fig. 2 in the limit of $s \to 0$. The vectors $\vec{r}_1$ and $\vec{r}_2$ are also shown in Fig. 2. Note that the points P_1 and P_2 are the *same* points in both Figs. 2 and 3; i. e., with respect to the boundary of each section of the body each point is at exactly the same location in both figures. It is clear from Fig. 2 that

$$\vec{r}_2' = \vec{r}_2 + \tfrac{1}{2}\vec{s} \tag{2.3a}$$

and

$$\vec{r}_1' = \vec{r}_1 - \tfrac{1}{2}\vec{s}, \tag{2.3b}$$

where

$$\vec{s} = s\vec{e}_z,$$

with $\vec{e}_z$ a unit vector in the z direction. From Figs. 2 and 3 and Eqs. (2.3) it follows that

$$\vec{r}' = \vec{r} + \vec{s}, \tag{2.4}$$

where the relative vectors $\vec{r}'$ and $\vec{r}$ are defined as

$$\vec{r}' = \vec{r}_2' - \vec{r}_1' \tag{2.5a}$$

and

$$\vec{r} = \vec{r}_2 - \vec{r}_1. \tag{2.5b}$$

We substitute Eq. (2.4) into Eq. (2.2) and form a power series expansion in s:

$$E = E_0 + E_1 s + \tfrac{1}{2}E_2 s^2 + \cdots . \tag{2.6}$$

Then from Eq. (2.1) we find that

$$F = -E_1. \tag{2.7}$$

For most of the standard functions $f(|\vec{r}_1' - \vec{r}_2'|)$ used in nuclear physics it is fairly easy to evaluate the quantity E_1 appearing in Eq. (2.7).

For ease of computation, it is helpful to convert the above double volume integrals into double surface integrals.[18] In the next two subsections we derive surface-integral expressions for the Coulomb and nuclear forces. The general form of these double surface integrals is

$$F = \oint_{S_1}\oint_{S_2} \{g_1(\vec{r})[(d\vec{S}_1\cdot\vec{e}_z)(d\vec{S}_2\cdot\vec{r}) + (d\vec{S}_1\cdot\vec{r})(d\vec{S}_2\cdot\vec{e}_z)] + g_2(\vec{r})(d\vec{S}_1\cdot\vec{r})(d\vec{S}_2\cdot\vec{r})\}, \tag{2.8}$$

where S_1 is the left-hand surface and S_2 is the right-hand surface. This formalism is completely general and applies to two touching bodies of arbitrary shape. For example, our equations apply to two touching spheres or spheroids. However, for the calculations reported in this paper we deal exclusively with shapes having flat touching surfaces, with nonzero neck radii.

It is helpful to categorize the contributions to the force from various parts of the surfaces of each body (assuming that the double volume integral has been converted into a double surface integral). We define $F(i,j)$ to be the contribution to F when $\vec{r}_1$ is on the left-hand surface labeled i and $\vec{r}_2$ is on the right-hand surface labeled j. The various labeled surfaces are shown in Fig. 1, and it is clear that the total interaction force at scission is given by

$$F = F(a,d) + F(a,c) + F(b,d) + F(b,c). \tag{2.9}$$

When $\vec{r}_1'$ is on surface b and $\vec{r}_2'$ is on surface c, $d\vec{S}_1$ and $d\vec{S}_2$ are both parallel to the unit vector $\vec{e}_z$ and, in the limit of $s \to 0$, $\vec{r} = \vec{r}_1 - \vec{r}_2$ is perpendicular to $\vec{e}_z$. Then from Eq. (2.8) we find that

$$F(b,c) = 0, \tag{2.10}$$

which reduces Eq. (2.9) to

$$F = F(a,d) + F(a,c) + F(b,d). \tag{2.11}$$

For *mass-symmetric fission* it follows from Eq. (2.8) that

$$F(a,c) = F(b,d), \tag{2.12}$$

and Eq. (2.11) simplifies to

$$F = F(a,d) + 2F(a,c). \tag{2.13}$$

B. Coulomb interfragment force

For the Coulomb interaction energy the appropriate scalar function in Eq. (2.2) is

$$f(|\vec{r}_1' - \vec{r}_2'|) = \rho_e^2/|\vec{r}_1' - \vec{r}_2'|, \tag{2.14}$$

where ρ_e is the charge density. Using the method outlined in the previous subsection, we obtain the result

$$F_C = \rho_e^2 \int_{V_1}\int_{V_2} d^3r_1 d^3r_2 \frac{z}{r^3}, \tag{2.15}$$

where $z = \vec{e}_z \cdot \vec{r}$.

One can verify easily the double-divergence relation

$$\frac{z}{r^3} = \frac{1}{6}\sum_{i,j=1}^{3} \frac{\partial}{\partial(r_1)_i}\frac{\partial}{\partial(r_2)_j} P_{ij}, \tag{2.16}$$

where

$$P_{ij} = \frac{1}{r}\left(\delta_{i,3}r_j + \delta_{j,3}r_i - \frac{z}{r^2}r_i r_j\right). \tag{2.17}$$

Then applying the divergence theorem twice to Eq. (2.15), we find that

$$F_C = \tfrac{1}{6}\rho_e^2 \oint_{S_1}\oint_{S_2} \frac{1}{r}\Big([(d\vec{S}_1\cdot\vec{e}_z)(d\vec{S}_2\cdot\vec{r}) + (d\vec{S}_1\cdot\vec{r})(d\vec{S}_2\cdot\vec{e}_z)] - \frac{z}{r^2}(d\vec{S}_1\cdot\vec{r})(d\vec{S}_2\cdot\vec{r})\Big), \tag{2.18}$$

which is in the form of Eq. (2.8).

Equation (2.18) can be derived by an alternative method, starting with the known double-surface expression for the Coulomb *interaction* energy,[17]

$$E_C = -\tfrac{1}{6}\rho_e^2 \oint_{S_1'}\oint_{S_2'} \frac{(d\vec{S}_1'\cdot\vec{r}')(d\vec{S}_2'\cdot\vec{r}')}{r'}. \tag{2.19}$$

We now substitute Eq. (2.4) into Eq. (2.19), make a power-series expansion of the form (2.6), and from Eq. (2.1) obtain Eq. (2.18). The advantage of this method is that we do not have to search for a double-divergence relation. Equation (2.16) was simple enough to derive for the Coulomb potential but analogous relations may be such more complicated for other types of potentials.

For axially symmetric shapes we present in Appendix A explicit expressions for $F_C(a,d)$ and $F_C(a,c)$, the contributions to the Coulomb force which were discussed in the previous subsection.

C. Nuclear interfragment force

We use an effective two-body potential of the form[2-4]

$$f(|\vec{r}_1' - \vec{r}_2'|) = -\frac{V_0}{4\pi\lambda^3}\frac{e^{-|\vec{r}_1'-\vec{r}_2'|/\lambda}}{|\vec{r}_1' - \vec{r}_2'|/\lambda}, \tag{2.20}$$

where λ is the range of the Yukawa interaction and V_0 is given by

$$V_0 = \frac{a_s\{1-\kappa[(N-Z)/A]^2\}}{\pi r_0^2 \lambda}.$$

Substituting Eq. (2.20) into Eq. (2.2) and expanding in powers of s by use of Eq. (2.4), we obtain from Eq. (2.1)

$$F_n = -\frac{V_0}{4\pi\lambda^3}\int_{V_1}\int_{V_2} d^3r_1 d^3r_2 \frac{e^{-r/\lambda}}{r^2} z\left(1+\frac{\lambda}{r}\right). \tag{2.21}$$

We now convert Eq. (2.21) into a double-surface integral. The simplest method, as indicated in the previous subsection, is to use the general expression for the nuclear *interaction* energy expressed as a double-surface integral[3,18]:

$$E_n = \frac{V_0}{4\pi\lambda^3}\oint_{S_1'}\oint_{S_2'} \frac{(d\vec{S}_1'\cdot\vec{r}')(d\vec{S}_2'\cdot\vec{r}')}{(r'/\lambda)^4} \times\left[\frac{r'}{\lambda} - 2 + \left(2+\frac{r'}{\lambda}\right)e^{-r'/\lambda}\right], \tag{2.22}$$

where r' is defined by Eq. (2.5a). As usual we expand Eq. (2.22) in powers of s and take the limit of $s \to 0$. This gives

$$F_n = -\frac{V_0\lambda}{4\pi}\oint_{S_1}\oint_{S_2}\frac{1}{r^4}\left\{[(\vec{S}_1\cdot\vec{e}_z)(d\vec{S}_2\cdot\vec{r}) + (d\vec{S}_1\cdot\vec{r})(d\vec{S}_2\cdot\vec{e}_z)]\left[\frac{r}{\lambda} + \left(2+\frac{r}{\lambda}\right)e^{-r/\lambda} - 2\right] - \frac{z}{\lambda^2}(d\vec{S}_1\cdot\vec{r})(d\vec{S}_2\cdot\vec{r}) \times\left[\frac{\lambda}{r}\left(3 - 8\frac{\lambda}{r}\right) + e^{-r/\lambda}\left(1 + 5\frac{\lambda}{r} + 8\frac{\lambda^2}{r^2}\right)\right]\right\}, \tag{2.23}$$

where r is defined by Eq. (2.5b). It is seen that this equation is of the form of Eq. (2.8).

For axially symmetric shapes we present in Appendix B explicit formulas for $F_n(a,d)$ and $F_n(a,c)$. Then in Appendix C we derive expressions for the nuclear interaction energy per unit area and force per unit area between two infinite parallel plates of finite thickness.

III. CALCULATED RESULTS

We now apply the formalism developed in Sec. II to some important problems in fission theory. In particular, for nuclei throughout the Periodic Table we calculate the interfragment force along dynamical paths leading from the fission saddle point. These paths are determined by solving classical equations of motion for a macroscopic system. The collective potential energy is calculated by means of a modified liquid-drop model that takes into account the lowering in the nuclear macroscopic energy due to the finite range of the nuclear force.[2-4] The collective kinetic energy is calculated for incompressiable, nearly irrotational hydrodynamical flow by use of the Werner-Wheeler method.[1,2] The Rayleigh dissipation function is calculated both for ordinary two-body visocosity[2,6,7] and for one-body dissipation, which occurs because of nucleons colliding with a moving potential wall[8-16] rather than with each other. As long as the total interfragment force remains attractive, we specify the nuclear shape in terms of smoothly joined portions of three quadratic surfaces of revolution.[1,2]

A. Two-body viscosity

We now present some detailed calculations for ^{236}U as functions of the two-body viscosity coefficient μ. As shown in Fig. 4, the neck ruptures when its radius is slightly less than 2 fm, with the precise value decreasing somewhat as μ increases. This occurs because of variations in the dynamical path due to changes in viscosity.[2] The nuclear system readjusts itself so as to lessen the amount of energy dissipation. As shown in Fig. 3 of Ref. 2, an increase in two-body viscosity produces a more elongated scission shape. This means in turn that as μ increases, the repulsive Coulomb force decreases relative to the attractive nuclear force. It is therefore necessary to proceed farther along the dynamical path to a smaller neck radius in order to reach a configuration at which the two forces are equal. Thus, as μ increases, the radius at which scission occurs decreases.

Because the shape is more compact at the time of neck rupture compared with a conventional zero-neck-radius scission configuration, the translational kinetic energy of the fission fragments at infinity is increased. We are not able to calculate the fission-fragment kinetic energy exactly, because this would entail introducing additional degrees of freedom to describe the healing of the neck after rupture, as well as calculating dynamically the postscission motion with this more-complicated shape parametrization. Instead, we describe the motion of the fission fragments from neck rupture

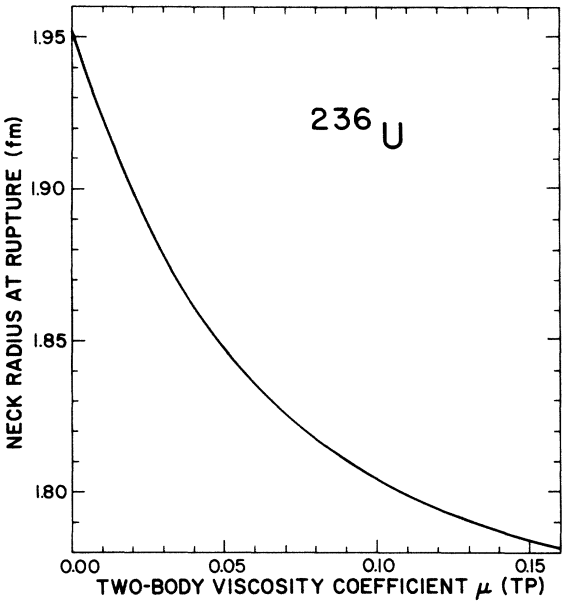

FIG. 4. Neck radius at rupture versus the two-body viscosity coefficient μ for the fission of ^{236}U. The initial conditions correspond to starting from the saddle point with 1 MeV of kinetic energy in the fission direction. The unit of viscosity is the terapoise (TP), where 1 TP $= 10^{12}$ P $= 10^{12}$ dyn s/cm^2 $= 6.24 \times 10^{-22}$ MeV s/fm^3 $= 0.948\hbar$/fm^3.

to infinity in terms of two spheroids with collinear symmetry axes.[2] The transition from the three-quadratic-surface parametrization to the two-spheroid parametization is accomplished by equating the values of two central moments and their corresponding time derivatives before and after neck rupture.[2]

We may estimate the uncertainty in the calculated final translational kinetic energy introduced by this approximation to the postscission motion. For the specific case of the fission of ^{236}U with a viscosity coefficient of 0.03 TP, the potential energy of the two-spheroid configuration is 4.7 MeV lower than the potential energy of the scission-point shape in the three-quadratic-surface shape parametrization. However, the error in the final kinetic energy is much less than this amount. Without solving the detailed equations of neck healing mentioned above, we wish to calculate the energy of translation acquired by the fragments after scission. In the simplest possible model, where we say that the final translational energy is the sum of the scission translational kinetic energy and the interaction energy of two spheres centered at the centers of mass of the real fragments,[1] we find $E_{\text{final}} = 164.2$ MeV. Another possible approximation is to assume that the fragments separate to infinity with the constant deformation they had at the scission

point (without replacing the fragments by spheroids; see again Fig. 1 for an illustration of such a shape). Here, the final energy is the sum of the interaction energy of the fragments at scission and the kinetic energy at scission, which in this case results in a prediction of 165.5 MeV for the final fragment kinetic energy. This approach is used for very dissipative systems (see Sec. III B). The model used in this paper, which is to add the translational energy acquired by the separating spheroids to the scission kinetic energy, gives 166.7 MeV for the final translational energy of the fragments. This approximation should slightly overestimate the final kinetic energy, since the two-spheroid model has much less nuclear (attractive) interaction energy than the exact scission shape, while having nearly the same Coulomb (repulsive) interaction energy. Thus, we would estimate the uncertainty in calculated final kinetic energy for this system to be of the order of 1–2 MeV, which is comparable to or less than the uncertainties in experimental values.

The fission-fragment kinetic energy calculated in this way for ^{236}U is shown in Fig. 5 as a function of the two-body viscosity coefficient μ. The calculated kinetic energy decreases with increasing viscosity for both a finite neck rupture and a conventional zero-neck-radius scission configuration, as indicated by the solid and dashed curves, respectively. This decrease arises from a combination of two effects. First, with increasing viscosity the system arrives at the scission configuration with less translational kinetic energy. Second, with increasing viscosity the scission configuration is more elongated, which decreases the Coulomb interaction energy and hence the post-scission contribution to the translational kinetic energy.

In Fig. 6 we show the neck radius at rupture as a function of $Z^2/A^{1/3}$ for various values of the two-body viscosity coefficient μ. The special methods used for treating the case of infinite viscosity are described in Ref. 2. For a given value of viscosity, the neck radius at scission increases as we proceed from light to heavy nuclei until we reach very heavy nuclei, where the radius begins to decrease slightly. This behavior arises because the Coulomb neck-rupture force is smaller for light nuclei than for heavy nuclei and because the macroscopic saddle-point shapes are different for light and heavy nuclei.[1-3] Light nuclei have dumbbell-like shapes while heavy nuclei have cylinder-like shapes. Very heavy nuclei have spheroidal or spherical saddle-point shapes. Thus, the delicate balance between the Coulomb and nuclear forces produces scission at a small radius for light nuclei and a larger radius for heavier nuclei. For a given medium-weight or heavy nucleus ($Z^2/A^{1/3} \gtrsim 800$), the neck radius decreases as μ increases. This behavior is reversed for lighter nuclei ($Z^2/A^{1/3} \lesssim 800$) and is associated with the rather abrupt transition[1,2] from

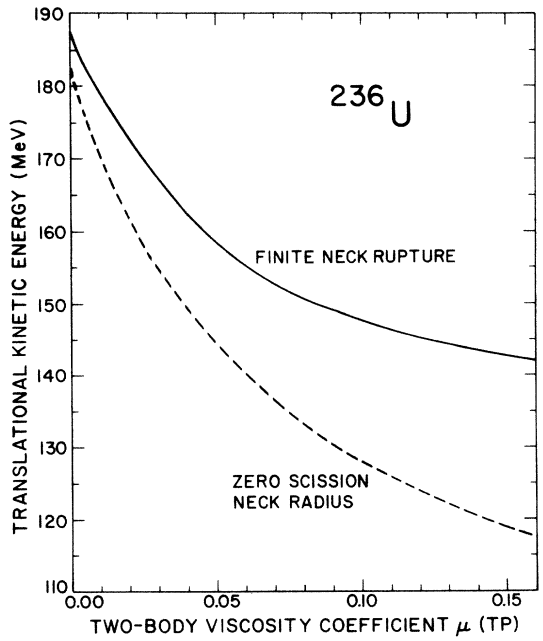

FIG. 5. Fission-fragment kinetic energy versus the two-body viscosity coefficient μ for the fission of ^{236}U. The solid curve is calculated for a finite neck rupture (see Fig. 4), and the dashed curve is calculated for a zero neck radius at scission (see Ref. 2).

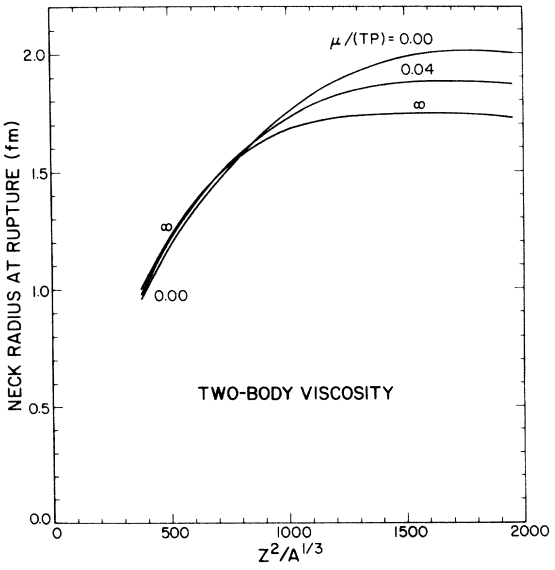

FIG. 6. Neck radius at rupture versus $Z^2/A^{1/3}$, for various values of the two-body viscosity coefficient μ.

dumbbell-like saddle-point shapes for light nuclei to cylinder-like saddle-point shapes for heavy nuclei. However, as shown in Fig. 6, this effect for light nuclei is very small.

The neck is sufficiently large at rupture to accommodate approximately two nucleons across its diameter for light nuclei and approximately three nucleons across its diameter for heavy nuclei. One sometimes attempts to estimate when neck rupture occurs on the basis of two or three particles across the diameter of the neck,[19,20] but such estimates depend upon the precise number of particles selected and neglect the variation with the size of the nucleus.

The calculated fission-fragment kinetic energy is shown in Fig. 7 as a function of $Z^2/A^{1/3}$ for various values of the two-body viscosity coefficient μ. This figure is analogous to Fig. 12 of Ref. 2, but includes the effect of the finite neck rupture on the calculated kinetic energy. (Although of little importance, for $\mu = \infty$ we here calculate the kinetic energy exactly by taking the sum of the Coulomb and nuclear interaction energies of the original fragments at scission rather than by approximating the postscission motion in terms of spheroidal fission fragments.) The dashed curves give the contributions to the kinetic energy acquired prior to neck rupture, which are somewhat smaller than the corresponding values for a zero scission neck radius given in Ref. 2. Nevertheless, the more-compact shapes at neck rupture lead to final kinetic energies that are always larger than those calculated for a zero scission neck radius. Therefore, to reproduce the same experimental data with the present calculations requires a larger two-body viscosity than with the earlier calculations.

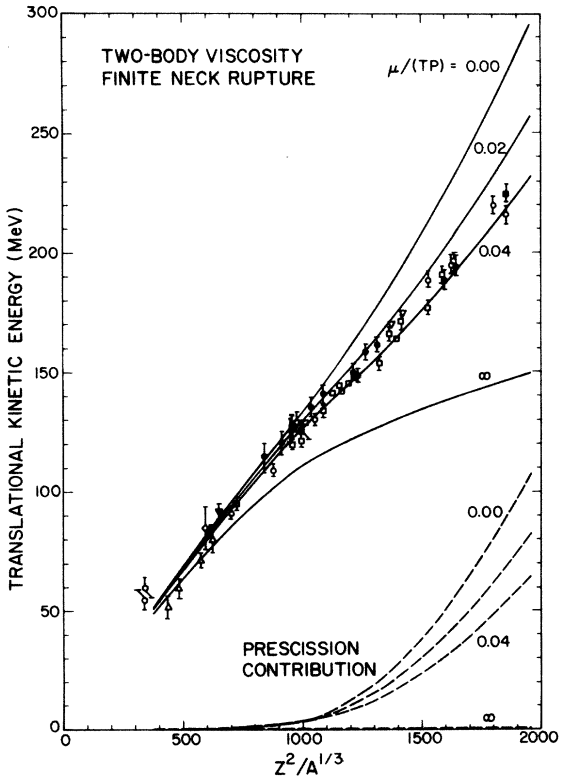

FIG. 7. Comparison of experimental most probable fission-fragment kinetic energies with results calculated for different values of the two-body viscosity coefficient μ (solid curves). The experimental data are for the fission of nuclei at high excitation energies, where the most probable mass division is into two equal fragments. The open symbols represent values for equal mass divisions only, and the solid symbols represent values averaged over all mass divisions. The experimental data are exactly the same as those in Fig. 12 of Ref. 2, where references to the appropriate experimental papers can be found. The dashed curves give the calculated translational kinetic energies acquired prior to neck rupture.

In particular, it is seen from Fig. 7 that the value

$$\mu = 0.03 \pm 0.01 \text{ TP}$$
$$= (19 \pm 6) \times 10^{-24} \text{ MeV s/fm}^3$$

accounts for most of the experimental data to within their uncertainties. As in Ref. 2, we place greater weight on the experimental data for lighter actinide nuclei than on that for very heavy nuclei. The present value is twice as large as the previous value of[2]

$$\mu = 0.015 \pm 0.005 \text{ TP}$$
$$= (9 \pm 3) \times 10^{-24} \text{ MeV s/fm}^3.$$

This large change in the value of μ arising solely from incorporating a finite neck rupture indicates the sensitivity of the results to the precise details of the model.

The value of the two-body viscosity coefficient that is required to critically damp the quadrupole oscillations of idealized nuclei is approximately 0.05 TP for heavy actinide nuclei and approximately 0.08 TP for medium-weight nuclei. Therefore, provided that nuclear dissipation arises from individual two-body collisions, the present study suggests that nuclear viscosity is about 60% as large as the critical value for quadrupole oscillations of actinide nuclei.

A comparison between the energy dissipated in microscopic and macroscopic calculations of the fission of ^{236}U resulted in a two-body viscosity coefficient of $\mu = 0.04$ TP,[21] which is larger than the original macroscopic value of $\mu = 0.015$ TP.[2] These estimates were made assuming a zero neck radius

at scission, and we have shown that the macroscopic value of μ increases when the finite rupture of the neck is taken into account. However, it can be seen from Ref. 21 that the microscopic estimate of μ also increases, by a factor of about 3, if it is assumed that scission takes place at a neck radius of about 1.9 fm. Therefore, the discrepancy between the microscopic and macroscopic values of μ is not removed by a finite-neck rupture.

B. One-body dissipation

We turn now to a similar study performed for one-body dissipation, in which the transfer of collective energy into internal energy proceeds by means of nucleons colliding with a moving potential wall[8-16] rather than with each other. For a system initially at rest in thermal equilibrium, the one-body dissipation rate is proportional to the integral over the nuclear surface of the square of the normal velocity of the surface. The constant of proportionality may be determined from a Fermi-gas model and corresponds to a highly over-damped system. The inertia may therefore be neglected in calculating the dynamical descent from the saddle point, and in analogy with previous dynamical calculations with one-body dissipation[14-16] we also make this excellent approximation here.

One-body dissipation has the opposite effect from two-body viscosity on the prescission dynamical path. In particular, whereas two-body viscosity shifts the dynamical path toward increased fragment elongation, one-body dissipation leads to a more compact scission configuration. In dynamical calculations involving a zero neck radius at scission,[14-16] it was found that without the use of any adjustable parameters one-body dissipation reproduces adequately the experimental kinetic energies for the fission of nuclei throughtout the Periodic Table, although for very heavy nuclei the calculated values are systematically higher than the experimental values by about 4%. It is our purpose here to see how a rupture at finite-neck radius modifies this result.

In Fig. 8 we show the neck radius at rupture as a function of $Z^2/A^{1/3}$. For heavy nuclei the radius at rupture is somewhat larger for one-body dissipation than for nonviscous flow. This is because the disruptive Coulomb force is larger for the compact shapes arising from one-body dissipation than for the more elongated shapes arising from nonviscous hydrodynamical flow.

In keeping with our approximation of neglecting the inertia, we calculate the kinetic energy of the fission fragments at infinity as the sum of the Coulomb and nuclear interaction energies at neck rupture (for the original fragments rather than for their equivalent spheroids). This would be strictly true if the dissipation were infinite, but represents an approximation here because of the healing of the neck in a finite time after rupture. We estimate the error of this approximation to be about 1–2 MeV. For the fission of ^{236}U with one-body dissipation, the final energy is calculated to be 176.9 MeV. This method underestimates the exact result, since neck healing will reduce the magnitude of the attractive nuclear interaction energy more than it does the repulsive Coulomb interaction energy. For comparison, we find the two-sphere approximation mentioned in Sec. III A predicts a final energy of 179.8 MeV.

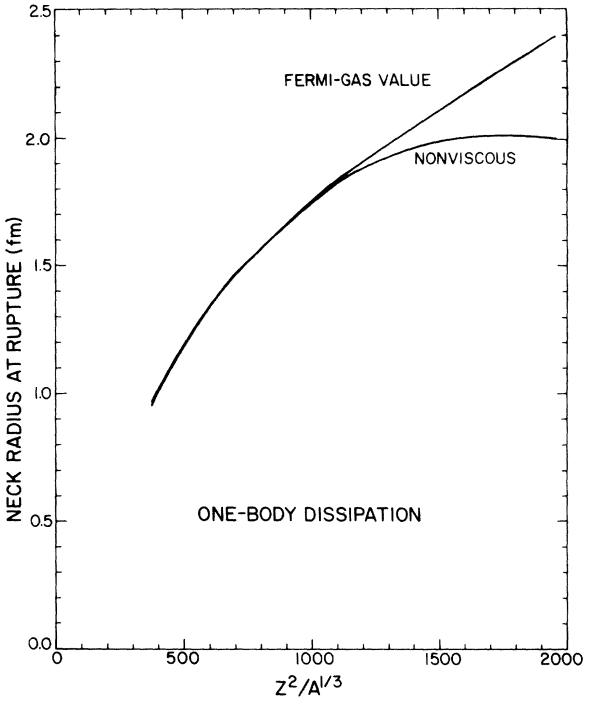

FIG. 8. Neck radius at rupture versus $Z^2/A^{1/3}$, for nonviscous hydrodynamical flow and also for one-body dissipation whose magnitude is obtained from a Fermi-gas model.

We show in Fig. 9 the fission-fragment kinetic energy calculated in this way as a function of $Z^2/A^{1/3}$. One-body dissipation reduces the kinetic energy compared to the result for nonviscous hydrodynamical flow given by the upper curve. This arises because of the nearly complete conversation of deformation energy into internal energy as the system descends from the fission saddle point to the point of neck rupture. Because of the compact shape at neck rupture, the postscission contribution to the kinetic energy is larger for one-body dissi-

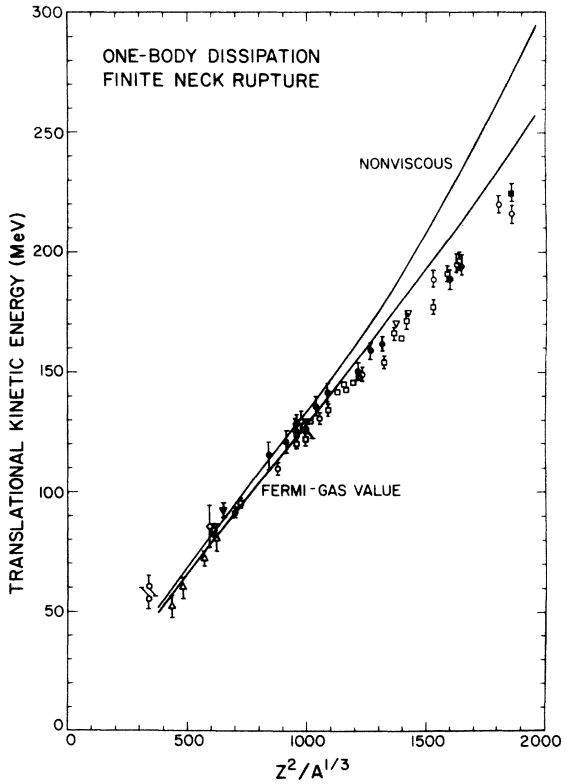

FIG. 9. Comparison of experimental most probable fission-fragment kinetic energies with results calculated for one-body dissipation whose magnitude is obtained from a Fermi-gas model. The experimental data are the same as in Fig. 7. The upper curve gives the result for nonviscous hydrodynamical flow.

pation than for nonviscous hydrodynamical flow, but the absence of an appreciable prescission contribution makes the total less. Compared with the result calculated previously for a zero neck radius at scission,[14-16] the kinetic energy calculated for a finite-neck rupture is somewhat higher. This arises because the shapes at the time of neck rupture are more compact and consequently have a higher Coulomb interaction energy than those with a zero neck radius at scission. The present calculated curve for one-body dissipation lies above the experimental values for heavy nuclei by about 8%. This is twice the discrepancy obtained previously for a zero neck radius at scission.[14-16]

IV. SUMMARY AND CONCLUSION

We have introduced a new degree of freedom to describe the rupture of the neck in nuclear fission. In particular, as the nucleus descends dynamically from its fission saddle point, we have calculated the Coulomb and nuclear interaction forces between the two portions of the nucleus and determined when they become equal in magnitude. We found in this way that the neck ruptures when its radius is about 2 fm for actinide nuclei and somewhat less for lighter nuclei.

We also calculated the translational kinetic energy of the fission fragments at infinity, taking into account the rupture of the neck at a finite radius. For each of two types of nuclear dissipation the calculated kinetic energies were compared with experimental values for the fission of nuclei throughout the Periodic Table. For ordinary two-body viscosity we found that the experimental kinetic energies are optimally reproduced when the viscosity coefficient μ has the value

$$\mu = 0.03 \pm 0.01 \text{ TP}$$

$$= (19 \pm 6) \times 10^{-24} \text{ MeV s/fm}^3,$$

which is twice the previous value determined on the basis of a zero neck radius at scission. For one-body dissipation we found that the calculated kinetic energies for heavy nuclei are about 8% larger than the experimental values, which is twice the previous discrepancy corresponding to a zero neck radius at scission.

In conclusion, the rupture of the neck at a finite radius plays an important role in the postscission dynamics of fission and in the conclusions to be drawn concerning nuclear dissipation. As we have shown, it is fairly easy to incorporate the effects of neck rupture into dynamical calculations of fission. Future studies of this type should take this important degree of freedom into account.

APPENDIX A: CONTRIBUTIONS TO THE COULOMB INTERFRAGMENT FORCE FOR AXIALLY SYMMETRIC SHAPES

We now present explicit formulas for $F_C(a,d)$ and $F_C(a,c)$ for the case of axially symmetric nuclear shapes. We first express Eq. (2.18) in cylindrical coordinates, with $\vec{r}_j = (\rho_j, \phi_j, z_j)$ for $j = 1, 2$. We may integrate immediately over one of the angles (either ϕ_1 or ϕ_2) to obtain a factor of 2π. The remaining angular integration is over the angle between the projections of $\vec{r}_1$ and $\vec{r}_2$ on the plane perpendicular to the axis of symmetry, which is taken to be the z axis. For the Coulomb potential this remaining angular integration can be performed explicitly, yielding various complete elliptic integrals.[1,17] Equation (2.18) is then expressed in the form of Eq. (2.11) or Eq. (2.13).

The contribution $F_C(a,d)$ can be written as

$$F_C(a,d)=\frac{4\pi}{3}\rho_e{}^2\int_{z_a^{\min}}^{z_a^{\max}}dz_a\int_{z_d^{\min}}^{z_d^{\max}}dz_d\,\frac{P_aP_d}{[(P_a+P_d)^2+(z_d-z_a)^2]^{1/2}}$$
$$\times\Bigg(\Bigg[2\frac{\partial P_a}{\partial z_a}\frac{\partial P_d}{\partial z_d}(z_d-z_a)-(P_a+P_d)\Big(\frac{\partial P_a}{\partial z_a}-\frac{\partial P_d}{\partial z_d}\Big)\Bigg]K(k_{ad})$$
$$+2\Big(P_a\frac{\partial P_a}{\partial z_a}-P_d\frac{\partial P_d}{\partial z_d}\Big)D(k_{ad})-\frac{(z_d-z_a)}{[(P_a+P_d)^2+(z_d-z_a)^2]}$$
$$\times\Bigg\{\frac{[-(P_a+P_d)^2+(P_a+P_d)(\partial P_d/\partial z_d-\partial P_a/\partial z_a)(z_d-z_a)+(\partial P_a/\partial z_a)(\partial P_d/\partial z_d)(z_d-z_a)^2]E(k_{ad})}{(1-k_{ad}^2)}$$
$$+2\frac{[(P_a+P_d)^2+[P_a(\partial P_a/\partial z_a)-P_d(\partial P_d/\partial z_d)](z_d-z_a)-2P_aP_d]}{(1-k_{ad}^2)}[K(k_{ad})-D(k_{ad})]$$
$$-4(P_aP_d/k_{ad}^2)[K(k_{ad})-2D(k_{ad})]\Bigg\}\Bigg), \tag{A1}$$

where P_a and P_d are the values of ρ on the surface at z_a and z_d, respectively,

$$k_{ad}{}^2=4P_aP_d/[(P_a+P_d)^2+(z_d-z_a)^2], \tag{A2}$$

$$D(k)=[K(k)-E(k)]/k^2, \tag{A3}$$

and $K(k)$ and $E(k)$ are the complete elliptic integrals of the first and second kinds, respectively. Notice that in Eq. (A1) there are two integrals over z, one for the region a and the other for the region d.

In the expression for $F_C(a,c)$ there is an integral over z for the region a and an integral over ρ_c from 0 to r_{neck}, the neck radius. The quantity z_c is fixed and is the value of z at which the system is divided into two portions. For $F_C(a,c)$ we obtain

$$F_C(a,c)=\frac{4\pi}{3}\rho_e{}^2\int_{z_a^{\min}}^{z_a^{\max}}dz_aP_a\int_0^{r_{\text{neck}}}d\rho_c\rho_c[(P_a+\rho_c)^2+(z_c-z_a)^2]^{-1/2}$$
$$\times\Bigg\{\Big[P_a+\rho_c+2\frac{\partial P_a}{\partial z_a}(z_c-z_a)\Big]K(k_{ac})-2\rho_cD(k_{ac})$$
$$+\frac{(z_c-z_a)^2}{(1-k_{ac}^2)}[(P_a+\rho_c)^2+(z_c-z_a)^2]^{-1}\Big[\Big(\frac{\partial P_a}{\partial z_a}(z_a-z_c)-P_a-\rho_c\Big)E(k_{ac})+2\rho_c[K(k_{ac})-D(k_{ac})]\Big]\Bigg\}, \tag{A4}$$

where

$$k_{ac}{}^2=4P_a\rho_c/[(P_a+\rho_c)^2+(z_c-z_a)^2]. \tag{A5}$$

The term $F_C(b,d)$ may be obtained by letting $a\to d$ and $c\to b$ in Eq. (A4). Equations (A1) and (A4) can be evaluated by Gaussian-Legendre quadrature.[1,17]

APPENDIX B: CONTRIBUTIONS TO THE NUCLEAR INTERFRAGMENT FORCE FOR AXIALLY SYMMETRIC SHAPES

For axially symmetric nuclear shapes Eq. (2.23) can be reduced to a three-dimensional integral. Unlike the expressions obtained in Appendix A for the Coulomb potential, here the second angular integration does not yield complete elliptic integrals and must be performed numerically.[3] For $F_n(a,d)$ we obtain

$$F_n(a,d)=-\frac{V_0}{2}\lambda\int_{z_a^{\min}}^{z_a^{\max}}dz_a\int_{z_d^{\min}}^{z_d^{\max}}dz_d\int_0^{2\pi}d\psi\,\frac{P_aP_d}{r_{ad}^4}$$
$$\times\Bigg\{\Big[P_a\frac{\partial P_d}{\partial z_d}-P_d\frac{\partial P_a}{\partial z_a}+2\frac{\partial P_a}{\partial z_a}\frac{\partial P_d}{\partial z_d}(z_d-z_a)+\Big(P_a\frac{\partial P_a}{\partial z_a}-P_d\frac{\partial P_d}{\partial z_d}\Big)\cos\psi\Big]\Big[\frac{r_{ad}}{\lambda}-2+\Big(2+\frac{r_{ad}}{\lambda}\Big)e^{-r_{ad}/\lambda}\Big]$$
$$-\frac{(z_d-z_a)}{\lambda^2}\Big[-P_aP_d(1+\cos^2\psi)+\Big(P_a\frac{\partial P_d}{\partial z_d}-P_d\frac{\partial P_a}{\partial z_a}\Big)(z_d-z_a)+\frac{\partial P_a}{\partial z_a}\frac{\partial P_d}{\partial z_d}(z_d-z_a)^2$$
$$+(P_a{}^2+P_d{}^2)\cos\psi+\Big(P_a\frac{\partial P_d}{\partial z_d}-P_d\frac{\partial P_a}{\partial z_a}\Big)(z_d-z_a)\cos\psi\Big]$$
$$\times\Big[\frac{\lambda}{r_{ad}}\Big(3-8\frac{\lambda}{r_{ad}}\Big)+\Big(1+5\frac{\lambda}{r_{ad}}+8\frac{\lambda^2}{r_{ad}^2}\Big)e^{-r_{ad}/\lambda}\Big]\Bigg\}, \tag{B1}$$

where

$$r_{ad} = [P_a^2 + P_d^2 - 2P_aP_d\cos\psi + (z_d - z_a)^2]^{1/2}. \tag{B2}$$

Similarly, for $F_n(a,c)$ we obtain

$$F_n(a,c) = -\frac{V_0}{2}\lambda \int_{z_a^{\min}}^{z_a^{\max}} dz_a P_a \int_0^{r_{\text{neck}}} d\rho_c \rho_c \int_0^{2\pi} d\psi r_{ac}^{-4}$$

$$\times \left\{ \left(2(z_c - z_a)\frac{\partial P_a}{\partial z_a} + P_a - \rho_c\cos\psi\right)\left[\frac{r_{ac}}{\lambda} - 2 + \left(2 + \frac{r_{ac}}{\lambda}\right)e^{-r_{ac}/\lambda}\right] \right.$$

$$\left. - \frac{(z_c - z_a)^2}{\lambda^2}\left((z_c - z_a)\frac{\partial P_a}{\partial z_a} + P_a - \rho_c\cos\psi\right)\left[\frac{\lambda}{r_{ac}}\left(3 - 8\frac{\lambda}{r_{ac}}\right) + \left(1 + 5\frac{\lambda}{r_{ac}} + 8\frac{\lambda^2}{r_{ac}^2}\right)e^{-r_{ac}/\lambda}\right]\right\}, \tag{B3}$$

where

$$r_{ac} = [P_a^2 + \rho_c^2 - 2P_a\rho_c\cos\psi + (z_c - z_a)^2]^{1/2}. \tag{B4}$$

Other notations are explained in Appendix A.

The term $F_n(b,d)$ may be obtained by letting $a \to d$ and $c \to b$ in Eq. (B3). Equations (B1) and (B3) can be evaluated by Gaussian-Legendre quadrature.[3,17,18]

APPENDIX C: NUCLEAR INTERACTION FORCES FOR TWO INFINITE PARALLEL PLATES

We now consider the example of two infinite parallel plates of width z_m that are separated by a distance s. We are especially interested in the limit of $s \to 0$ in order to verify Eqs. (2.21) and (2.23).

For this configuration the total nuclear interaction energy is infinite, so we consider instead the interaction energy per unit area. From Eqs. (2.2) and (2.20) it follows that the interaction energy per unit area is

$$\mathcal{E}_n(s) = -\tfrac{1}{2}\lambda V_0 e^{-s/\lambda}(1 - e^{-z_m/\lambda})^2, \tag{C1}$$

which reduces to

$$\mathcal{E}_n(s) \to -\tfrac{1}{2}\lambda V_0 e^{-s/\lambda} \tag{C2}$$

as $z_m \to \infty$.

Then from Eqs. (2.1) and (C1) we find that at contact the attractive nuclear force per unit area is

$$\mathcal{F}_n = -\tfrac{1}{2}V_0(1 - e^{-z_m/\lambda})^2, \tag{C3}$$

which reduces to

$$\mathcal{F}_n \to -\tfrac{1}{2}V_0 \tag{C4}$$

as $z_m \to \infty$. Equation (C3) can also be obtained directly from Eq. (2.21) by means of a few simple manipulations. Alternatively, one can obtain Eq. (C3) from the double-surface expression of Eq. (2.23), but this is a more laborious derivation.

*This research was sponsored by the U.S. Energy Research and Development Administration under contracts with Union Carbide Corporation and the University of California.

†Present address: Department of Astronomy and Astrophysics, The University of Chicago, Chicago, Illinois 60637.

[1]J. R. Nix, Nucl. Phys. A130, 241 (1969); Lawrence Berkeley Laboratory Report No. UCRL-17958, 1968 (unpublished).

[2]K. T. R. Davies, A. J. Sierk, and J. R. Nix, Phys. Rev. C 13, 2385 (1976).

[3]H. J. Krappe and J. R. Nix, in *Proceedings of the Third International Atomic Energy Agency Symposium on the Physics and Chemistry of Fission, Rochester, New York, 1973* (International Atomic Energy Agency, Vienna, 1974), Vol. 1, p. 159.

[4]J. R. Nix and A. J. Sierk, Phys. Scr. 10A, 94 (1974).

[5]J. Błocki, J. Randrup, W. J. Swiatecki, and C. F. Tsang, Lawrence Berkeley Laboratory Report No. LBL-5014, 1976 (unpublished).

[6]J. Schirmer, S. Knaak, and G. Süssmann, Nucl. Phys. A199, 31 (1973).

[7]R. Wieczorek, R. W. Hasse, and G. Süssmann, in *Proceedings of the Third International Atomic Energy Agency Symposium on the Physics and Chemistry of Fission, Rochester, New York, 1973* (see Ref. 3), Vol. I, p. 523.

[8]C. Toepffer, in *Proceedings of the International Conference on Reactions between Complex Nuclei, Nashville, Tennessee, 1974*, edited by R. L. Robinson, F. K. McGowan, J. B. Ball, and J. H. Hamilton (North-Holland, Amsterdam/American Elsevier, New York, 1974), Vol. 1, p. 129.

[9]G. Wegmann, Phys. Lett. 50B, 327 (1974).

[10]G. Wegmann, in Proceedings of the International Workshop III on Gross Properties of Nuclei and Nuclear Excitations, Hirschegg, Kleinwalsertal, Austria, 1975, edited by W. D. Myers [Technische Hocheschule Darmstadt Report No. AED-Conf.-75-009-000, 1975 (unpublished)], p. 28.

[11]D. H. E. Gross, Nucl. Phys. A240, 472 (1975).

[12]W. J. Swiatecki, Lawrence Berkeley Laboratory Report No. LBL-4296, 1975 (unpublished).
[13]J. Randrup, in Proceedings of the International Workshop IV on Gross Properties of Nuclei and Nuclear Excitations, Hirschegg, Kleinwalsertal, Austria, 1976 [Technische Hochschule Darmstadt Report No. AED-Conf-76-015-000, 1976 (unpublished)], p. 69.
[14]W. D. Myers, in Proceedings of the International Workshop IV on Gross Properties of Nuclei and Nuclear Excitations Hirschegg, Kleinwalsertal, Austria, 1976 (see Ref. 13), p. 86.
[15]A. J. Sierk and J. R. Nix, in Proceedings of the Symposium on Macroscopic Features of Heavy-Ion Collisions, Argonne, Illinois, 1976 [Argonne National Laboratory Report No. ANL/PHY-76-2, 1976 (unpublished)], Vol. I, p. 407.
[16]J. Błocki *et al.*, Lawrence Berkeley Laboratory report (unpublished).
[17]K. T. R. Davies and A. J. Sierk, J. Comp. Phys. 18, 311 (1975).
[18]K. T. R. Davies and J. R. Nix, Phys. Rev. C 14, 1977 (1976).
[19]P. Möller (private communication).
[20]M. G. Mustafa (private communication).
[21]S. E. Koonin and J. R. Nix, Phys. Rev. C 13, 209 (1976).